Journal of chemical & engineering data

Article

Cite This: J. Chem. Eng. Data 2020, 65, 1051−1059

pubs.acs.org/jced

Molecular Dynamics Study on the Adsorption of UO_2^{2+} from an Aqueous Phase: Effect of Grafting Dibenzo Crown Ether and Dicyclohexano Crown Ether on the Polystyrene Surface

Praveenkumar Sappidi and Jayant K. Singh*

Computational Nano Science Laboratory, Department of Chemical Engineering, Indian Institute of Technology (IIT) Kanpur, Kanpur 208016, India

Supporting Information

ABSTRACT: Atomistic molecular dynamics (MD) simulations are performed in order to understand the adsorption behavior of UO_2^{2+} ions from an aqueous medium. The dibenzo crown ether (DBCE) and dicyclo hexano crown ether (DCHCE) grafted on the polystyrene surface is used as the adsorbent. We investigated the role of grafting density ρ_s (mol/nm^2) of DBCE and DCHCE on the adsorption behavior with increasing UO_2^{2+} ion concentration C_s (M). The amount of adsorption (q_e) (mg/g) increases with an increase in UO_2^{2+} salt concentration and follows the Langmuir adsorption isotherm model. The maximum amount of adsorption (q_{max}) (mg/g) increases with increasing grafting density for both DBCE and DCHCE. The DCHCE shows higher q_{max} values compared to DBCE over the entire range of ρ_s: 0.25 mol/nm^2 < ρ_s < 2.07 mol/nm^2. Overall, q_{max} show a 5-fold increase for DBCE and DCHCE with an increase in ρ_s from 0.25 mol/nm^2 to 2.07 mol/nm^2. The optimum ρ_s for the maximum adsorption is found to be 1.25 mol/nm^2 for both DBCE and DCHCE. The dynamical behavior of the adsorbed UO_2^{2+} is also investigated by calculating the self-diffusion coefficient (D) and mean residence time (τ). The D value decreases by ∼47% for DBCE and ∼61% for DCHCE, for the entire range of ρ_s, with an increase in C_s. Similarly, the τ value shows more than a 5-fold increase irrespective of grafting densities for both DBCE and DCHCE with increasing C_s. In the end, we investigate the UO_2^{2+} binding structure with DBCE and DCHCE. The potential of mean force (PMF) analysis shows a favorable free-energy for the binding of UO_2^{2+} to DCHCE compared to DBCE.

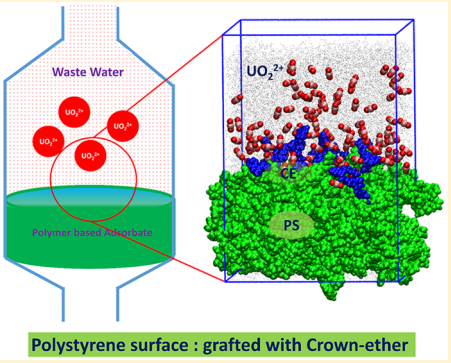

1. INTRODUCTION

Separation of lanthanides and actinides from aqueous waste or radioactive waste is a global problem. Radioactive waste associated with actinides such as uranium (U) would lead to the long-term hazard for the geosphere and biosphere. In nuclear wastewater, the presence of uranyl ion (UO_2^{2+}) can be absorbed by the living organism, and thereby these ions can interact with bicarbonate anions and plasma proteins in the blood.[1] Further, these uranyl ions can be retained in the bone or in lungs, liver, and kidneys, which can cause several health problems such as renal damage and cancer.[2] Therefore, the World Health Organization (WHO) has set the threshold limit for uranium concentration as 0.0015 mg/L in drinking water.[3] Nevertheless, the recovery of uranium from aqueous waste or nuclear waste would also be economically beneficial as it is a useful resource for nuclear energy generation.

Various methods have been used to remove or extract the UO_2^{2+} from aqueous waste, such as chemical precipitation,[4] reverse osmosis, solvent extraction,[5] and ion exchange.[6] However, these methods have drawbacks, such as the generation of a secondary pollutant which is challenging to handle. There are other conventional methods such as ultrafiltration[7] and nanofiltration.[8] These methods have limitations such as high cost, high energy, and inefficiency at a low metal ion concentration. In the recent past, adsorption techniques are being used.[9−11] These adsorption methods are easy to operate, highly efficient, low cost and also allow the recovery at a low concentration of metal ions; hence, the adsorption method is one of the most common methods employed for the removal of an impurity from an aqueous phase.

The various inorganic materials such as metal oxides, mesoporous carbons, silica gel, and natural minerals have been used effectively for the removal of UO_2^{2+} from aqueous waste.[1,12] However, these materials have drawbacks such as low surface area, irregular pose size, and poor selectivity and are limited to specific metal ions and in general these are toxic in nature.[1] This difficulty supersedes with the use of the polymer-based adsorbents. The polymers possessing specific chelate groups can bind the metal ions. The polymer-based adsorbate materials have advantages such as high uptake and selectivity and are less harmful to the environment.[13] The

Special Issue: Hans Hasse

Received: May 26, 2019
Accepted: July 23, 2019
Published: August 5, 2019

DOI: 10.1021/acs.jced.9b00462
J. Chem. Eng. Data 2020, 65, 1051−1059

metal chelating agents grafted on the polymer based solid phase adsorbents have been used previously for the adsorption of UO_2^{2+}.[14,15] Ilayaraja et al.[14] showed a significant increase in the UO_2 adsorption capacity by using the polyamido amine (PAMAM) dendrite grafted on the surface of polystyrene divinylbenzene. Further, these types of materials can be used for simultaneous desorption and adsorption. Annam et al.[15] have recently studied the carboxy methylphosphine oxide (CMPO) cross-linked with polyethylene glycol (PEG) and dimethacrylate (DMA) for the adsorption of uranium. This material provides a good adsorption and desorption behavior and also has a high radiolytic stability.[15] Further, polymer substrates as adsorbents are preferred due to their reusability at high acidic conditions.[14,15]

Pederson[16] first discovered crown ethers. These crown ethers possess the intriguing metal ion binding complexation property in their cavity. Zolotov[17] observed that polymerized crown ether enhances the adsorption of uranyl ions from the seawater using the metal binding reaction. The free-energy analysis suggests that the binding of UO_2^{2+} onto dibenzo crown ether (DBCE) and dicyclohexano crown ether (DCHCE) is favorable among the various crown ethers available.[17,18] Thus, DBCE and DCHCE would be ideal candidates for the adsorption of UO_2^{2+} ions. The UO_2^{2+} binding or adsorption on the crown ethers have laid important understanding as these ions show competitive interactions with the solvent molecules and crown ethers.[19] Mohite et al.[20] observed that polymerizing the DBCE amplifies the UO_2^{2+} adsorption, which also provides advantages such as high resistance to an acidic medium and easy to handle. Bey et al.[21] showed a thermodynamically stronger complexation or binding of metal ions to the cavity of the polymerized crown ether when compared to the bare crown ether. In the recent MD simulation studies,[22,23] polystyrene (PS) grafted DBCE and DCHCE have shown a favorable 3-fold increase in the binding free-energy of gadolinium (Gd^{3+}) and UO_2^{2+} to the DBCE and DCHCE. The optimum crown ether grafting density (ρ_s) mol/nm^2 on the polystyrene surface is found to be 1.25 mol/nm^2 for the adsorption of Gd^{3+} from the aqueous solution as evident from recent molecular dynamics (MD) simulations and verified with the experimental studies.[24]

Despite all the literature available on adsorption UO_2^{2+} from the aqueous waste, there are a few questions which need to be answered. How the polystyrene surface grafted with crown ethers influence the adsorption of UO_2^{2+} from an aqueous medium? What is the role of chemically different crown ethers on adsorption behavior. What is the optimum grafting or (coating) density (ρ_s) of crown ethers on the polymer beads? In this article, we aim to address these unanswered questions using molecular simulations.

2. METHODOLOGY AND SIMULATION DETAILS

We have considered two crown ethers DBCE and DCHCE for grafting onto the polystyrene surface. The initial structures for DBCE, DCHCE, and PS are taken from our earlier work.[22−24] First, we create an amorphous polymer surface equivalent to the experimental density.[25] The details of the generation of an amorphous polymer surface are provided in previous work.[24] However, brief information is provided in Figure S1 in the Supporting Information. The molecular geometry and partial atomic charge calculation of the DBCE and DCHCE are performed by ChelpG scheme using density function theory calculations using Gaussian09 with B3LYP/6-31 G(d,p).[26] The conformations of both DB18C6 and DCH18C6 were optimized by complexation with UO_2^{2+} as described in our earlier work.[22,23] These optimized crown ether molecules are grafted randomly on the polystyrene surface similar to the earlier work[24] and generated two sets of initial configurations, one for grafting DBCE and another for DCHCE. The grafting of the DBCE and DCHCE on the PS surface was performed using a methylated bond by randomly replacing the para hydrogens of the polystyrene. This is performed in such a way that DBCE and DCHCE molecules were exposed in the z-direction. The schematic representation of the crown ether grafting on the PS is shown in Figure S2. Each grafted substrate is subjected to the variation of grafting densities (ρ_s) as 0.24, 0.49, 0.74, 1.00, 1.25, 1.66, and 2.07 mol/nm^2, which are equivalent to the grafting of 3, 6, 9, 12, 15, 20, and 25 molecules, respectively. Figure 1a illustrates the grafted surface

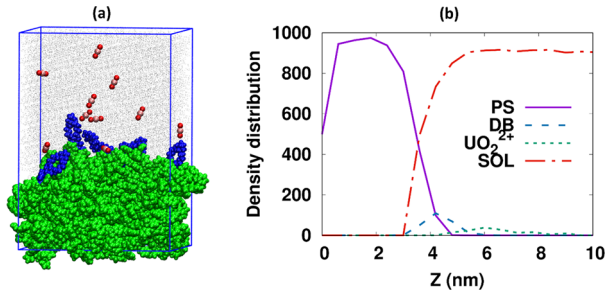

Figure 1. (a) Initial simulation setup at a grafting density 0.25 mol/nm^2 on the surface of the polystyrene. (b) Initial density distribution along the z-direction of the initial simulation setup. Color codes: green, polystyrene; blue, crown ether (DBCE); red, uranyl oxygens; pink, uranium; and gray, water molecules.

of polystyrene. Figure 1b presents the initial density distribution of all molecules present in the system. These grafted substrates are used as starting configurations for investigating the adsorption behavior of UO_2^{2+} in water.

The OPLS force-field[27] is used for modeling DBCE, DCHCE, PS, HNO_3, UO_2^{2+}, and NO_3^-. The detailed information on the force-field is given in earlier works.[22,23] The atomic charges of all molecules are taken from previous work.[22,23] Tables 1 and 2 present the bonded and nonbonded interactions, respectively. The water molecules are modeled using the TIP3P water model.[28] The 1 M acidic medium is maintained by explicitly considering the H_3O^+ and NO_3^- ions in an aqueous solution. The box dimensions of 7.06 nm × 7.06 nm × 10 nm are used for filling water and salt ions above the grafted substrate. To avoid a periodic image effect, we have added an additional 20 nm vacuum slab on this prepared system. The electrostatics are calculated using the particle mesh Ewald (PME)[29] with the cutoff radius as 1.2 nm. The van der Waals interactions are calculated using a Lennard−Jones 6-12 potential with a cutoff radius of 1.2 nm. The LINCS[30] method is used for constraining the bond lengths. The temperature at 300 K and pressures at 1 bar are maintained using a Nosé−Hoover thermostat and a Parrinello−Rahman barostat. The equation of motion is solved using the leapfrog algorithm with a 2 fs time step. The energy minimization is performed using the steepest descent method. Gromacs 4.5.5[31] is used for all MD simulations. NVT-MD simulations are run for 40 ns, and thermodynamic analysis is performed on the last 10 ns trajectory. The uncertainties were calculated using one standard deviation of the averaged

DOI: 10.1021/acs.jced.9b00462
J. Chem. Eng. Data 2020, 65, 1051−1059

Table 1. Force Field Parameters Comprising of Harmonic Bond Stretching, Angle Bending, and Torsional Rotation for Crown Ethers[a]

bonds	$b_{i,0\,(1)}$ (nm)	$k_{b,i\,(2)} \times 10^{-6}$ (kJ/mol nm^4)
H−C	0.10800	284512.0
C−C	0.15220	265265.6
C−O	0.13640	376560.0
H−C (PS)	0.10800	284512.0
C−C (PS)	0.15220	265265.6
O−U (UO_2)	0.18000	209200.0
O−N (NO_3)	0.12600	125520.0
H−O (H_3O)	0.09450	462750.0
angles	$\theta_{i,0\,(3)}$ (deg)	$k_{\theta,i\,(4)}$(kJ/mol rad^2)
H−C−H	109.450	306.4
H−C−C	109.450	366.9
H−C−O	109.500	292.880
C−C−O	121.400	669.440
C−C−H	109.450	366.9
C−O−C	116.900	694.544
C−C−C	120.000	376.6
C−C−C (PS)	109.450	482.3
C−C−H (PS)	109.450	306.4
H−C−H (PS)	109.450	306.4
O−U−O (UO_2)	180.000	627.6
O−N−O (NO_3)	120.000	627.6
H−O−H (H_3O)	104.500	418.4

dihedrals	C0 (kJ/mol)	C1 (kJ/mol)	C2 (kJ/mol)	C3 (kJ/mol)	C4 (kJ/mol)	C_5(kJ/mol)
C−C−O−C	5.23000	7.32200	−12.5520	0.00000	0.00000	0.00000
C−O−C−C	1.71544	2.84512	1.04600	−5.60656	0.00000	0.00000
O−C−C−C	2.87441	0.58158	2.09200	−5.54799	0.00000	0.00000
O−C−C−O	−1.15060	1.15060	0.00000	0.00000	0.00000	0.00000
C−C−C−C	0.52719	−6.39734	−1.69452	7.56467	0.00000	0.00000
C−O−C−H	1.58992	4.76976	0.00000	−6.35968	0.00000	0.00000
H−C−C−O	0.97905	2.93716	0.00000	−3.91622	0.00000	0.00000
H−C−C−H	0.66525	1.99576	0.00000	−2.66102	0.00000	0.00000
H−C−C−C	0.76567	2.29701	0.00000	−3.06269	0.00000	0.00000
C−C−C−C (PS)	16.02681	−4.39111	−14.0289	2.39325	0.00000	0.00000
H−C−C−H (PS)	0.66525	1.99576	0.00000	−2.66102	0.00000	0.00000
C−C−C−H (PS)	0.76567	2.29701	0.00000	−3.06269	0.00000	0.00000

[a]Here (1) equilibrium bond length, (2) bond length force constant, (3) equilibrium bond angle, and (4) bond angle force constant. The parameters $b_{i,0}$, $\theta_{i,0}$, k_b, k_θ are the reference values for bond length, bond angle, force constants for bond stretching, bond angles, respectively. The C_0, C_1, C_2, C_3, C_4, and C_5 are the dihedral coefficients.

Table 2. Lennard−Jones Interaction Parameters for All Atoms of Crown Ethers, UO_2, and NO_3[a]

atom	σ (Å)	ε (kJ/mol)
C	3.50	2.76×10^{-1}
H	2.50	1.25×10^{-1}
O	2.90	5.85×10^{-1}
U (UO_2)	3.35	0.11×10^{0}
O (UO_2)	2.85	1.83×10^{0}
N (NO_3)	3.12	6.69×10^{-1}
O (NO_3)	2.94	6.27×10^{-1}

[a]σ is the distance where interaction energy is zero, and ε is the potential well depth.

property, i.e., with 68% confidence level, by splitting 10 ns sampling time into 5 blocks based on earlier work.[32]

To understand the free-energy barriers associated with UO_2^{2+} binding to the crown ether, we have performed the Umbrella Sampling (US) analysis using a harmonic biased potential, as shown in eq 1,

$$w_i(\xi) = \frac{1}{2}k(\xi - \xi_i)^2 \quad (1)$$

Here, the collective variable (ξ) is the distance between the center of the mass of crown ether and UO_2^{2+} ion (only one ion). ξ_i is the variation in the reaction coordinate from the DBCE or DCHCE, and k is the biasing force constant. The harmonic potential with a force constant of 1000 (kJ/mol nm^2) is used to restrain the UO_2^{2+} along the normal to the center of mass of DBCE and DCHCE. The weighted histogram analysis method (WHAM)[33,34] is used to calculate the potential of mean force (PMF) as implemented in Gromacs.[35] A total of 23 windows simulations are performed for each case, viz., DBCE-UO_2^{2+} in (1) water and (2) vacuum and similarly DCHCE-UO_2^{2+} in (3) water and (4) vacuum. Each window simulation is run for 10 ns. A total of 92 window simulations are performed. The Langmuir isotherm model is used for performing the adsorption analysis of UO_2^{2+} using the equation given as

DOI: 10.1021/acs.jced.9b00462
J. Chem. Eng. Data 2020, 65, 1051−1059

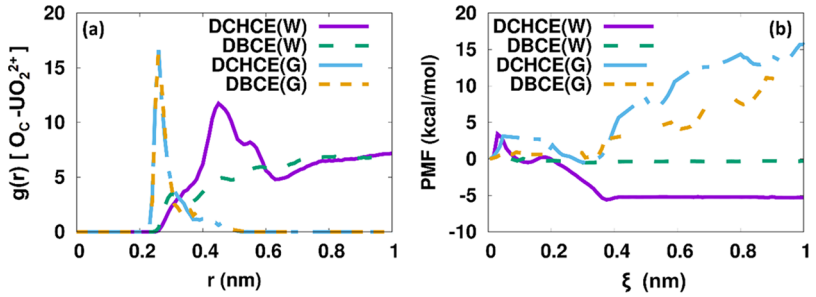

Figure 2. (a) Radial distribution function of O_C and UO_2^{2+} in water and in vacuum for DBCE and DCHCE and (b) PMF curves for the ion binding energy along the z direction. The statistical error values are <0.6% for all the PMF data.

$$q_e = \frac{q_{max} KC}{1 + KC} \quad (2)$$

where q_e is the amount of UO_2^{2+} adsorbed per unit mass of adsorbent (i.e., DBCE or DCHCE) (mg/g). The q_{max} (mg/g) is the maximum amount of UO_2^{2+} ions adsorbed, K is the Langmuir constant, and C (mol/L) is the equilibrium UO_2^{2+} ion concentration. The Langmuir model equilibrium parameter is defined as R_L, which is given by the following relation:

$$R_L = \frac{1}{1 + KC} \quad (3)$$

The Einstein relation is used for calculating the self-diffusion coefficient of UO_2^{2+}.[24]

3. RESULTS AND DISCUSSION

3.1. UO_2^{2+} Binding Structure. The radial distribution function (RDF) between UO_2^{2+} and the oxygens of the crown ethers (O_C) for both DBCE and DCHCE is calculated to observe the UO_2^{2+} ion binding behavior. Figure 2a presents the RDF plots of UO_2^{2+}–O_C for both DBCE and DCHCE in the gas and solvent phases. In the gas phase, the first peak of UO_2^{2+}–O_C RDF is located at 0.24 nm, while in water the peak slightly shifts to 0.48 nm. The UO_2^{2+}–O_C showed a more prominent peak for DCHCE compared to DBCE in the aqueous phase; however, there is no difference seen in the gas phase. The binding distance between UO_2^{2+}–O_C in the aqueous phase is 2 times higher than the gas phase (vacuum). The observed peak positions in the gas phase are in line with the results reported by Shamov et al.,[36] where a UO_2^{2+}–O_C binding distance of 0.24 nm is reported. In aqueous solutions, the UO_2^{2+}–O_C (18C6) peak is located at around ∼0.42 nm as reported by Guilbaud and Wipff.[37] The increased binding distance between UO_2^{2+}–O_C in water is due to the presence of solvent molecules and other ions. This behavior is in line with earlier reported studies.[36,37] Furthermore, it is evident from Figure 2a that DCHCE shows more complexation of UO_2^{2+} compared to the DBCE in water.

The structural differences between the UO_2^{2+} and crown ethers in the gas phase and solvent phase are further understood by evaluating the potential of mean force (PMF) using the Umbrella Sampling technique. Figure 2b presents the PMF curves of UO_2^{2+}-DBCE and UO_2^{2+}-DCHCE for the gas phase (G) and water phase (W). The minimum free-energy is found to be −0.51 kcal/mol at ∼0.30 nm in the gas phase and −5.60 kcal/mol at ∼0.38 nm in the aqueous phase for UO_2^{2+}-DCHCE. Similarly, for the case of UO_2^{2+}-DBCE, the free-energy minimum is found to be −0.88 kcal/mol at ∼0.24 nm in the gas phase and −0.49 kcal/mol at ∼0.39 nm in the solvent phase. In an aqueous solution, the DCHCE shows more favorable binding free-energy for UO_2^{2+} compared to the gas phase. Overall, the binding of UO_2^{2+} to the crown ether follows the order: DCHCE (w) < DBCE (w) in water and DBCE (g) < DCHCE (g) in gas, based on the values of PMFs. To confirm this, we have performed gas phase DFT calculations to see the binding behavior. The binding energies (at 0 K) of UO_2^{2+} with DBCE were −269.08 kcal/mol and −16.18 kcal/mol in gas and solvent phases, respectively. As expected, it is found that binding energies are significantly lower in the solvent phase as compared to the binding energies in the gas phase. However, in MD simulations the free-energy shows different behavior than DFT, which primarily could be due to the force-field employed in this work and/or difference in conditions such as temperature and highly acidic medium. We observe an over 10-fold higher free-energy for UO_2^{2+}-DCHCE binding in the aqueous phase compared to the gas phase. These results are in accordance with the observed structural differences. The effect of the phenyl group for the binding energy of UO_2^{2+} to crown ether is well reported in the literature.[22,23] It is observed that the binding free energy becomes favorable with an increase in the phenyl group. Furthermore, for ions binding with the crown ether, it has been shown earlier[22,23] that the electrostatic contribution is significantly more than that due to the dispersive van der Waals interactions. The next section describes the adsorption behavior of UO_2^{2+} ions.

3.2. Adsorption Behavior. Figure 3 presents the UO_2^{2+} ion density profiles along the normal to the PS surface for the maximum crown ether grafting density at ρ_s = 2.07 mol/nm^2. The UO_2^{2+} ion density profiles for other ρ_s are provided in Figures S3 and S4. The significant peak is located at ∼4.8 nm on the normal (z) to the grafted substrate for both DBCE and DCHCE. The peak position does not change with the increase in grafting density and salt concentration. With the increase in

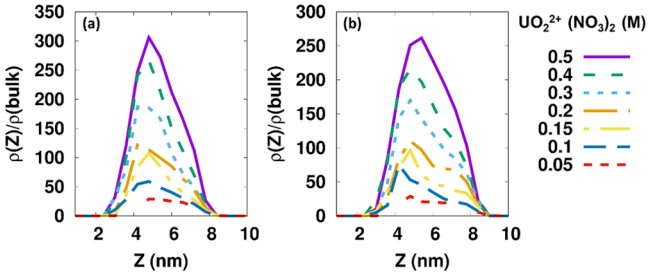

Figure 3. Density distribution of UO_2^{2+} at ρ_s = 2.07 mol/nm^2 for (a) DBCE and (b) DCHCE.

DOI: 10.1021/acs.jced.9b00462
J. Chem. Eng. Data 2020, 65, 1051−1059

salt concentration, the intensity of the peak shows an increasing behavior, which is seen for all the cases of ρ_s studied here. This broad peak indicates significant binding between the UO_2^{2+} and crown ethers (DBCE and DCHCE). Figure 4 presents the snapshots of UO_2^{2+} binding to both

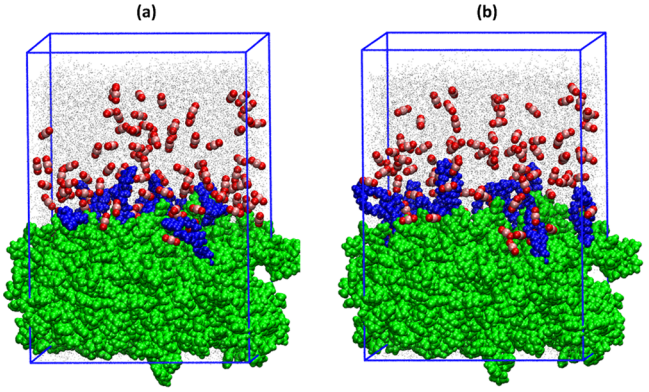

Figure 4. Snapshot of adsorbed UO_2^{2+} ions on the surface of grafted crown ether molecules at 0.5 M $UO_2^{2+}(NO_3)_2$ at ρ_s = 2.07 mol/nm^2: (a) DBCE and (b) DCHCE.

DBCE and DCHCE. It is observed that UO_2^{2+} directly binds in the cavity of the crown ether. The UO_2^{2+} ions first fill the void spaces available above the substrate and subsequently condense near the vicinity of the crown ethers. Then, the ions near the substrate agglomerate themselves due to the electrostatic interactions. These agglomerations of UO_2^{2+} ions lead to the formation of a thick layer of width ∼2 nm in the *z*-direction above the crown ether is grafted PS surface.

Figure 5 presents the adsorption isotherm curves of UO_2^{2+} ions. We have calculated the amount adsorbed UO_2^{2+} ions q_e (mg/g) by considering a monolayer thickness of 1 nm above the PS surface. It is observed that the adsorption curves follow the Langmuir adsorption isotherm model. The q_e shows an increasing behavior with the increase in UO_2^{2+} $(NO_3)_2$ salt concentration over the entire range ($0.25 < \rho_s < 2.07$ mol/nm^2). This increasing behavior is seen until the ρ_s = 1.67 mol/nm^2, beyond which the q_e does not show any significant change for both the crown ethers. However, the maximum value of q_e is seen at ρ_s = 2.07 mol/nm^2 for DCHCE and DBCE.

Figure 6 presents the behavior of q_{max} with the variation in ρ_s. The eq 2 is used for the calculation of the maximum adsorption capacity (q_{max}). Overall, q_{max} increases with

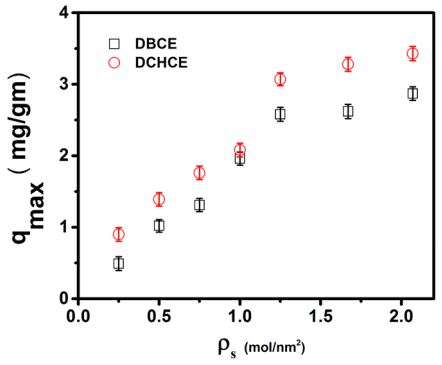

Figure 6. Maximum amount adsorption q_{max} (mg/g) of UO_2^{2+} ions with an increase in grafting density. The statistical errors are <6%.

increasing ρ_s. The DCHCE show higher adsorption of UO_2^{2+} compared to DBCE over the entire range of ρ_s studied. In the case of DCHCE-coated PS, the maximum adsorption of UO_2^{2+} is found to be ∼3.43 mg/g. On the other hand, in the case of DBCE-coated PS, the corresponding amount is ∼2.87 mg/g. The observed q_{max} values are in a similar order of magnitude when compared to other solid-based adsorbents.[38,39] For instance, the batch column study by Chen et al.[38] showed a q_{max} value of 0.2021 mg/g using the phosphate rock apatite (PRA) as the adsorbate. Sun et al.[39] recently showed significant enhancement of q_{max} (∼8.06 mg/g) with chitosan modified phosphate rock (CPR).

In this work, q_{max} increases by ∼485% and ∼281% for DBCE and DCHCE, respectively, with an increase in ρ_s from 0.25 to 2.07 mol/nm^2. Furthermore, it is observed that q_{max} increase by ∼11% for both DBCE and DCHCE in the higher range, 1.25 mol/nm^2< ρ_s < 2.07 mol/nm^2. In the intermediate range, 0.25 mol/nm^2< ρ_s < 1.25 mol/nm^2, q_{max} increases by ∼425% and ∼240% for DBCE and DCHCE, respectively. It is also seen from Figure 6 that q_{max} does not show any significant variation at ρ_s > 1.25 mol/nm^2. Based on the above observations, ρ_s = 1.25 mol/nm^2 is deduced as the optimum grafting density for crown ether on the PS substrate for both DBCE and DCHCE for maximizing the adsorption capacity of UO_2^{2+}. Interestingly, the optimum ρ_s value observed in this work is similar to the earlier work for adsorption on Gd^{3+} ions.[24]

Figure 7 presents the Langmuir equilibrium parameter (R_L) calculated using eq 3 at different ρ_s values. The R_L show a decrease from 0.5 to 0.05 with an increase in the salt concentration for both DBCE and DCHCE. However, no significant difference is seen for the entire range of ρ_s. This

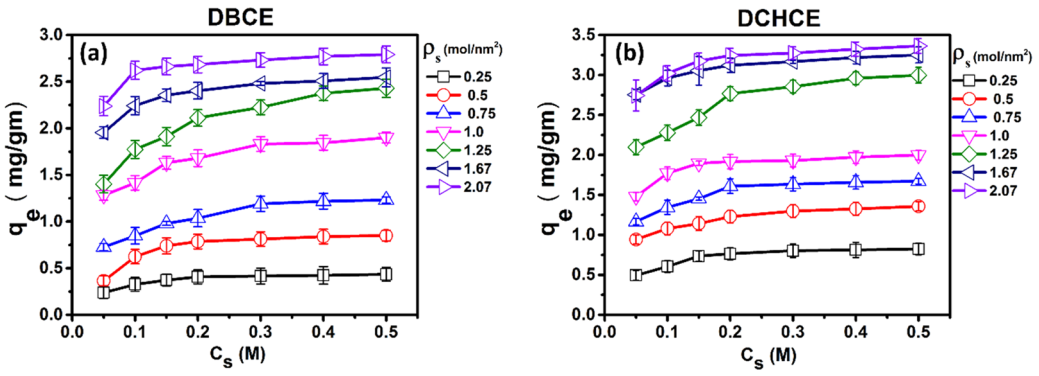

Figure 5. Amount of adsorption q_e (mg/g) of UO_2^{2+} ions for PS surface grafted with (a) DBCE and (b) DCHCE. The statistical errors are <4%.

DOI: 10.1021/acs.jced.9b00462
J. Chem. Eng. Data 2020, 65, 1051−1059

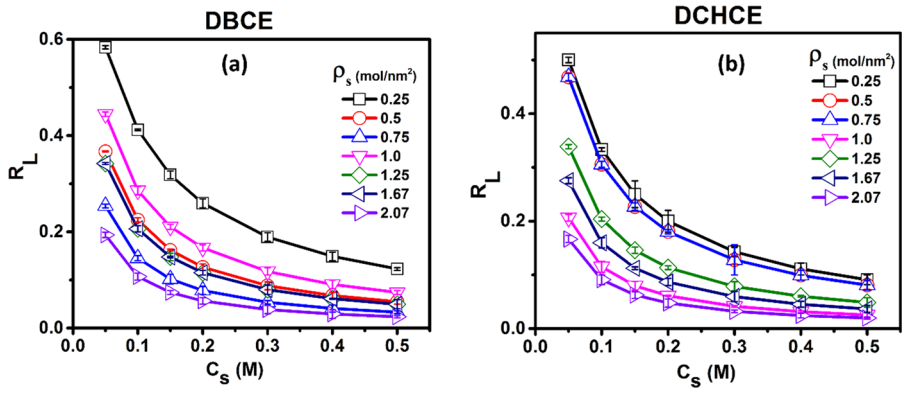

Figure 7. Langmuir model equilibrium parameter (R_L): (a) DBCE and (b) DCHCE. The statistical errors are <4%.

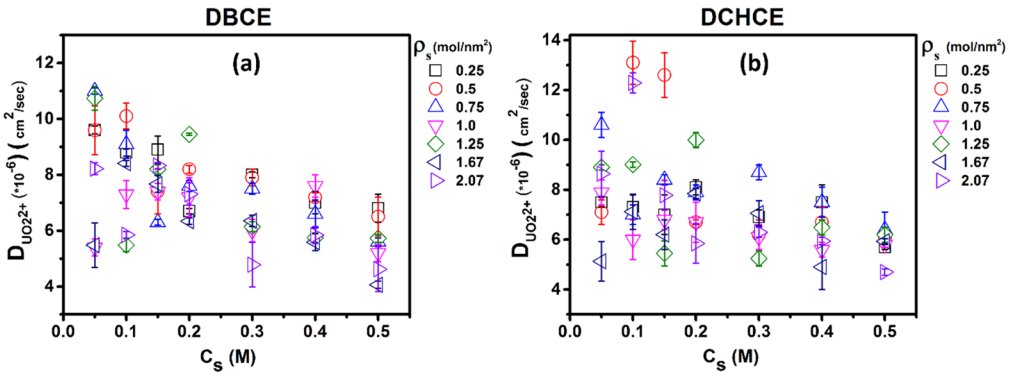

Figure 8. Adsorbed UO_2^{2+} ions self-diffusion coefficient: (a) DBCE and (b) DCHCE. The maximum error of 13% is seen in the data.

Table 3. Mean Residence Time τ (ps) of Adsorbed UO_2^{2+} Ions at Different ρ_s Values[a]

	ρ_s(mol/nm^2)						
C_s (M)	0.25	0.5	0.75	1.0	1.25	1.67	2.07
				τ (ps) for DBCE grafting			
0.05	155.3 (9)	211.6 (9)	105.0 (11)	107.8 (5)	291.2 (10)	319.5 (5)	257.4 (8)
0.1	195.9 (8)	228.9 (10)	223.7 (9)	255.5 (7)	366.1 (5)	437.0 (8)	384.7 (6)
0.15	279.0 (9)	207.2 (7)	183.4 (6)	417.8 (7)	362.4 (8)	659.7 (7)	493.5 (8)
0.2	389.9 (7)	344.4 (8)	456.2 (7)	390.1 (7)	416.3 (9)	780.0 (6)	782.3 (7)
0.3	425.5 (8)	523.7 (8)	672.4 (7)	412.5 (6)	628.1 (6)	777.0 (6)	796.2 (5)
0.4	805.3 (7)	491.4 (7)	857.5 (7)	359.2 (8)	726.2 (5)	846.0 (5)	677.3 (6)
0.5	840.0 (7)	557.9 (6)	888.1 (6)	428.1 (5)	913.4 (6)	932.6 (4)	631.5 (4)
				τ (ps) for DCHCE Grafting			
0.05	183.9 (7)	203.8 (7)	192.3 (10)	128.5 (8)	149.1 (9)	223.9 (5)	272.2 (8)
0.1	180.5 (7)	241.1 (13)	210.6 (7)	323.2 (6)	444.2 (9)	357.7 (7)	235.8 (12)
0.15	106.5 (7)	325.6 (12)	274.1 (8)	366.5 (7)	745.7 (5)	421.5 (6)	353.6 (8)
0.2	152.4 (8)	209.4 (7)	323.9 (8)	353.1 (7)	737.5 (10)	439.2 (7)	335.4 (6)
0.3	197.7 (7)	302.7 (6)	284.5 (9)	455.0 (6)	779.9 (5)	471.3 (7)	416.6 (6)
0.4	219.5 (7)	475.6 (7)	345.6 (7)	490.0 (6)	844.6 (6)	555.1 (5)	683.3 (6)
0.5	377.4 (6)	538.5 (6)	351.9 (6)	503.8 (6)	848.0 (6)	530.7 (6)	734.5 (5)

[a]The error values in the brackets represent one standard deviation of the block average.

behavior of R_L indicates that adsorption is favorable at a high salt concentration (i.e., 0.5 M) for both grafted crown ethers (DBCE and DCHCE). It is observed that the R_L value shows similar behavior at high ρ_s values of 1.67 and 2.07 mol/nm^2, which is an indicative of the saturation of crown ether grafting density.

3.3. UO_2^{2+} Diffusion. Figure 8 presents the UO_2^{2+} ion self-diffusion (D) behavior, calculated using the Einstein relation. The D value show a decreasing nature with increasing C_s and ρ_s. The highest and lowest values of D are seen as 11×10^{-6} cm^2/s and 4.06×10^{-6} cm^2/s (at ρ_s = 0.75 mol/nm^2, C_s = 0.05 M) and (at ρ_s = 1.75 mol/nm^2, C_s = 0.5 M), respectively, for the case of DBCE grafted PS. Similarly, for the case of DCHCE grafted PS, the highest and lowest values of D are 13×10^{-6} cm^2/s and 4.7×10^{-6} cm^2/s (at ρ_s = 0.5 mol/nm^2, C_s = 0.05 M) and (at ρ_s = 2.07 mol/nm^2, C_s = 0.5 M), respectively. The observed D values from our simulation is 2-orders less than that of UO_2^{2+} ion diffusion in the bulk water ($\sim 4.3 \times 10^{-4}$ cm^2/s).[40] The previous experiments[41] report that the D values as $\sim 4.7-3.9 \times 10^{-4}$ cm^2/s for the uranyl sulfate

DOI: 10.1021/acs.jced.9b00462
J. Chem. Eng. Data 2020, 65, 1051−1059

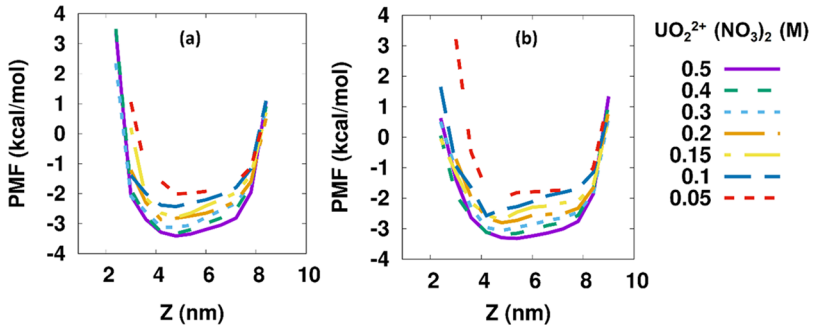

Figure 9. PMF profiles of adsorbed UO_2^{2+} ions on the surface of grafted crown ether molecules at 0.5 M $UO_2^{2+}(NO_3)_2$ at ρ_s = 2.07 mol/nm^2: (a) DBCE and (b) DCHCE.

concentration as 0.1−0.5 M. The recent simulation study[42] showed a good estimation of the effect of water model on the uranyl ion diffusion and overall D values match with that from the experiments. This is attributed to the enhanced adsorption of UO_2^{2+} on the crown ether grafted substrates. Overall, the D value of UO_2^{2+} ion reduces by ∼47% and ∼61% for the case of DBCE-PS and DCHCE-PS, with increasing C_s for the entire range of ρ_s. Thus, it is clear that grafting of DBCE slightly lowers the dynamics of UO_2^{2+} compared to the case of DCHCE.

3.4. UO_2^{2+} Ion Residence Time. The mean residence time τ (ps) of adsorbed UO_2^{2+} ions calculated using an exponential fit of an occupational time correlation $C(t)$, given as[42,43]

$$C(t) = \frac{\langle \sum_{i=1}^{N} \varphi_i(t_0)\varphi_i(t + t_0)\rangle}{\langle \sum_{i=1}^{N} \varphi_i(t_0)\varphi_i(t_0)\rangle} \quad (4)$$

where, $\varphi_i(t_0)$ is taken to be 1 if the UO_2^{2+} is adsorbed on the crown ether, otherwise it is zero. Table 3 reports the τ (ps) values of UO_2^{2+} ions. It is observed that τ values increase with an increase in C_s. At ρ_s = 1.25 mol/nm^2, the maximum rise of τ is seen from 291 to 913 ps, for DBCE, and 149 to 848 ps for DCHCE, with an increase in C_s. Overall, with an increase of C_s and ρ_s, more than a 5-fold increase in the τ value is seen. This behavior indicates a significant rise in adsorption behavior with an increase in C_s and ρ_s. The saturation of τ value is seen at ρ_s > 1.25 mol/nm^2 for both DBCE and DCHCE. This behavior is similar to the earlier studies on Pd^{2+} adsorption on the poly(amidoamine) PAMAM dendrites grafted on graphene and functionalized carbon nanotubes.[44,45] In a similar study on Gd^{3+} adsorption, the τ value show a 3-fold increase with the increase in $(Gd^{3+}(NO_3)_3)$ salt concentration and grafting density of crown ether (DBCE and DCHCE).[24] It is noted that with an increase in $(UO_2^{2+}(NO_3)_2)$ salt concentration, 2-fold higher τ values for UO_2^{2+} are observed compared to the τ values of Gd^{3+} studied.[24] The binding free energy of UO_2^{2+} with crown ether in water is −5.60 kcal/mol for UO_2^{2+}-DCHCE and −0.49 kcal/mol for UO_2^{2+}-DBCE. From our earlier work,[24] the binding free energy of Gd^{3+} and crown ether in water is −2.02 kcal/mol for Gd^{3+}-DCHCE and −0.42 kcal/mol for Gd^{3+}-DBCE. Thus, based on the binding free-energy values, we believe that the adsorption of UO_2^{2+} on the crown ether grafted PS substrate is more prominent compared to that of Gd^{3+}.

3.5. Potential of Mean Force (PMF). Figure 9 presents the PMF curves of UO_2^{2+} adsorption for both DBCE and DCHCE at ρ_s = 2.07 mol/nm^2. The PMF is calculated using the relation: PMF $(Z) = -KT \ln(\rho(z)/\rho(\text{bulk}))$. The location of PMF minima does not change with an increase in C_s and ρ_s. The PMF curves at different ρ_s values are given in Figures S5 and S6. The minimum PMF value of −3.7 kcal/mol is seen at z = 0.48 nm and C_s = 0.5 M for DBCE. On the other hand, the minimum PMF value of −3.4 kcal/mol is seen at z = 0.51 nm and C_s = 0.5 M for DCHCE. The PMF minima values do not change significantly at ρ_s > 1.25 mol/nm^2 for the case of both DBCE and DCHCE at C_s = 0.5 M. The observed PMF values are favorable for the adsorption behavior for both DBCE and DCHCE. The PMF minima locations seen in Figure 9 are similar to the binding distance between uranyl ion (UO_2^{2+})−O_C for DCHCE and DBCE as observed in Figure 2a. It is observed from Figure 9 and Figures S4 and S5 that PMF values do not show significant variation with an increase in grafting density. The PMF values are similar in order for both DBCE and DCHCE. In the PMF calculation using MD, we use a larger system consisting of salt and acidic medium, which is different from the binding energy calculation performed using the Umbrella Sampling technique, as shown in section 3.1, which is only for a single ion. These PMF values show a good qualitative agreement with the previous simulations on Gd^{3+} adsorption on DBCE and DCHCE grafted PS substrate.[24] Overall, from our results the UO_2^{2+} show a (∼6%) lower free-energy of binding compared to Gd^{3+} for both DBCE and DCHCE.[24] Using the free-energy values for both cases, it is understood that the adsorption of UO_2^{2+} is slightly more favorable when compared to the Gd^{3+}.

4. CONCLUSION

The MD simulations are performed to understand the UO_2^{2+} from the aqueous waste by varying the effect of crown ether (DBCE and DCHCE) grafting density (ρ_s). The amount of adsorption (q_e) shows an increase with an increase in C_s and ρ_s. The maximum amount of adsorption (q_{max}) (mg/g) show an increase with ρ_s for both DBCE and DCHCE. The maximum q_{max} values, ∼2.87 mg/g for DBCE and ∼3.47 mg/g for DCHCE, are observed at ρ_s = 2.07 mol/nm^2. These q_{max} values show a qualitatively good agreement with the experiments on similar type of adsorbents. The DCHCE show higher q_{max} values when compared to DBCE over the entire range of ρ_s. Overall the q_{max} values show an ∼485% increase for DBCE and ∼281% increase for DCHCE with an increase in ρ_s from 0.25 to 2.07 mol/nm^2. Furthermore, in the higher range of ρ_s (1.25 mol/nm^2 < ρ_s < 2.07 mol/nm^2) we have found q_{max} increases by ∼11% for both DBCE and DCHCE. The ρ_s value of 1.25 mol/nm^2 is deduced as the optimum grafting density for crown ether on the PS substrate for both DBCE and DCHCE for maximizing the adsorption capacity of UO_2^{2+}. The

DOI: 10.1021/acs.jced.9b00462
J. Chem. Eng. Data 2020, 65, 1051−1059

self-diffusion coefficient (D) of UO_2^{2+} shows a decrease as ∼47% for DBCE and ∼61% for DCHCE in the range of ρ_s varying from 0.25 to 2.07 mol/nm^2, with more than a 5-fold increase in mean residence time (τ) values with an increase in ρ_s from 0.25 to 2.07 mol/nm^2. The observed PMF values are in good agreement with the binding structure and binding energy values of UO_2^{2+}-crown ether (DBCE and DCHCE). Thus, we believe that this work is able to provide molecular insights into the crown ether coated PS-based material for uranyl adsorption.

■ ASSOCIATED CONTENT

Supporting Information

The Supporting Information is available free of charge on the ACS Publications website at DOI: 10.1021/acs.jced.9b00462.

Simulation snapshots of the creation of polymer surface and description, density distribution, and PMF curves (PDF)

■ AUTHOR INFORMATION

Corresponding Author

*Phone: 91-512-259 6141 (office). Fax: 91-512-259 0104. E-mail: jayantks@iitk.ac.in.

ORCID

Jayant K. Singh: 0000-0001-8056-2115

Notes

The authors declare no competing financial interest.

■ ACKNOWLEDGMENTS

This work is supported by the Board of Research on Nuclear Sciences (BRNS), Department of Atomic Energy (DAE), and Government of India, Sanction No. 36(1)/14/02/2015-BRNS/100. We are grateful to HPC, IIT Kanpur for the computational support. P.K.S. gratefully acknowledges the Science and Engineering Research Board (SERB), Department of Science and Technology (DST), Government of India for the National Post-Doctoral Fellowship (Grant PDF/2017/000121).

■ REFERENCES

(1) Gao, M.; Zhu, G.; Gao, C. A review: adsorption materials for the removal and recovery of uranium from aqueous solutions. *Energy Environ. Focus* **2014**, *3*, 219−226.

(2) Manaka, M.; Seki, Y.; Okuzawa, K.; Watanabe, Y. Uranium sorption onto natural sediments within a small stream in central Japan. *Limnology* **2008**, *9*, 173−183.

(3) Berlin, M.; Zalups, R. K.; Fowler, B. A. Mercury. In *Handbook on the Toxicology of Metals*; Academic Press Publishers, 2007; 943 pages.

(4) Santos, E. A.; Ladeira, A. C. Recovery of uranium from mine waste by leaching with carbonate-based reagents. *Environ. Sci. Technol.* **2011**, *45*, 3591−3597.

(5) Koh, M.; Yoo, J.; Park, Y.; Bae, D.; Park, K.; Kim, H.; Kim, H. Supercritical CO_2 extraction of Uranium (VI) from HNO_3 eolution esing N, N, N′, N′-Tetrabutyl-3-oxapentanediamide. *Ind. Eng. Chem. Res.* **2006**, *45*, 5308−5313.

(6) Bae, S. Y.; Southard, G. L.; Murray, G. M. Molecularly imprinted ion exchange resin for purification, preconcentration and determination of UO_2^{2+} by spectrophotometry and plasma spectrometry. *Anal. Chim. Acta* **1999**, *397*, 173−181.

(7) Semião, A. J.; Rossiter, H. M.; Schäfer, A. I. Impact of organic matter and speciation on the behaviour of uranium in submerged ultrafiltration. *J. Membr. Sci.* **2010**, *348*, 174−180.

(8) Khedr, M. G. Radioactive contamination of groundwater, special aspects and advantages of removal by reverse osmosis and nanofiltration. *Desalination* **2013**, *321*, 47−54.

(9) Hua, M.; Zhang, S.; Pan, B.; Zhang, W.; Lv, L.; Zhang, Q. Heavy metal removal from water/wastewater by nanosized metal oxides: a review. *J. Hazard. Mater.* **2012**, *211*, 317−331.

(10) Ni, Y.; Jin, L.; Zhang, L.; Hong, J. Honeycomb-like Ni@ C composite nanostructures: synthesis, properties and applications in the detection of glucose and the removal of heavy-metal ions. *J. Mater. Chem.* **2010**, *20*, 6430−6436.

(11) Tripathi, A.; Melo, J. S.; D'Souza, S. F. Uranium (VI) recovery from aqueous medium using novel floating macroporous alginate-agarose-magnetite cryobeads. *J. Hazard. Mater.* **2013**, *246*, 87−95.

(12) Chen, L.; Xin, H.; Fang, Y.; Zhang, C.; Zhang, F.; Cao, X.; Zhang, C.; Li, X. Application of metal oxide heterostructures in arsenic removal from contaminated water. *J. Nanomater.* **2014**, *2014*, 1−10.

(13) Metilda, P.; Gladis, J. M.; Venkateswaran, G.; Rao, T. P. Investigation of the role of chelating ligand in the synthesis of ion-imprinted polymeric resins on the selective enrichment of uranium (VI). *Anal. Chim. Acta* **2007**, *587*, 263−271.

(14) Ilaiyaraja, P.; Singha Deb, A. K.; Sivasubramanian, K.; Ponraju, D.; Venkatraman, B. Adsorption of uranium from aqueous solution by PAMAM dendron functionalized styrene divinylbenzene. *J. Hazard. Mater.* **2013**, *250-251*, 155−166.

(15) Annam, S.; Brahmmananda Rao, C.V.S.; Sivaraman, N.; Sivaramakrishna, A.; Vijayakrishna, K. Carbamoylmethylphosphine oxide functionalised porous crosslinked polymers towards sequential separation of uranium (VI) and thorium (IV). *React. Funct. Polym.* **2018**, *131*, 203−210.

(16) Pedersen, C. J. Cyclic polyethers and their complexes with metal salts. *J. Am. Chem. Soc.* **1967**, *89*, 7017−7036.

(17) Zolotov, I. A. *Macrocyclic Compounds in Analytical Chemistry*; Wiley: Chicago, IL, 1997.

(18) Servaes, K.; De Houwer, S.; Görller-Walrand, C.; Binnemans, K. Spectroscopic properties of uranyl crown ether complexes in non-aqueous solvents. *Phys. Chem. Chem. Phys.* **2004**, *6*, 2946−2950.

(19) Agrawal, Y. K.; Shrivastav, P.; Menon, S. K. Solvent extraction, separation of uranium (VI) with crown ether. *Sep. Purif. Technol.* **2000**, *20*, 177−183.

(20) Mohite, B. S.; Jadhav, A. S. Column chromatographic separation of uranium (VI) and other elements using poly (dibenzo-18-crown-6) and ascorbic acid medium. *J. Chromat. A* **2003**, *983*, 277−281.

(21) Bey, A.; Dreyer, O.; Abetz, V. Thermodynamic analysis of alkali metal complex formation of polymer-bonded crown ether. *Phys. Chem. Chem. Phys.* **2017**, *19*, 15924−15932.

(22) Sappidi, P.; Namsani, S.; Ali, S. M.; Singh, J. K. Extraction of Gd^{3+} and UO_2^{2+} Ions Using Polystyrene Grafted Dibenzo Crown Ether (DB18C6) with Octanol and Nitrobenzene: A Molecular Dynamics Study. *J. Phys. Chem. B* **2018**, *122*, 1334−1344.

(23) Sappidi, P.; Mir, S. H.; Singh, J. K. Effect of polystyrene length for the extraction of Gd^{3+} and UO_2^{2+} ions using dicyclohexano crown ether (DCH18C6) with octanol and nitrobenzene: A molecular dynamics study. *J. Mol. Liq.* **2018**, *271*, 166−174.

(24) Sappidi, P.; Boda, S.; Ali, S. M.; Singh, J. K. Adsorption of gadolinium (Gd3+) ions on the di benzo crown ether (DBCE) and di cyclo hexano crown ether (DCHCE) grafted on the polystyrene surface: insights from all atom molecular dynamics simulations and experiments. *J. Phys. Chem. C* **2019**, *123*, 12276−12285.

(25) Zoller, P.; Walsh, D. J.*Standard Pressure-Volume-Temperature Data for Polymers*; CRC Press, 1995; p 412

(26) Frisch, M. J.; Trucks, G. W.; Schlegel, H. B.; Scuseria, G. E.; Robb, M. A.; Cheeseman, J. R.; Nakatsuji, H.et al. *Gaussian 09*, revision D. 01; Gaussian Inc.: Wallingford, CT, 2009.

(27) Jorgensen, W. L.; Maxwell, D. S.; Tirado-Rives, J. Development and testing of the OPLS all-atom force field on conformational energetics and properties of organic liquids. *J. Am. Chem. Soc.* **1996**, *118*, 11225−11236.

DOI: 10.1021/acs.jced.9b00462
J. Chem. Eng. Data 2020, 65, 1051−1059

(28) Jorgensen, W. L.; Chandrasekhar, J.; Madura, J. D.; Impey, R. W.; Klein, M. L. Comparison of simple potential functions for simulating liquid water. *J. Chem. Phys.* **1983**, *79*, 926−935.
(29) Darden, T.; York, D.; Pedersen, L. Particle mesh Ewald: An N·log (N) method for Ewald sums in large systems. *J. Chem. Phys.* **1993**, *98*, 10089−10092.
(30) Hess, B.; Bekker, H.; Berendsen, H. J.; Fraaije, J. G. LINCS: a linear constraint solver for molecular simulations. *J. Comput. Chem.* **1997**, *18*, 1463−1472.
(31) Pronk, S.; Páll, S.; Schulz, R.; Larsson, P.; Bjelkmar, P.; Apostolov, R.; Shirts, M. R.; Smith, J. C.; Kasson, P. M.; van der Spoel, D.; Hess, B.; Lindahl, E. GROMACS 4.5: a high-throughput and highly parallel open source molecular simulation toolkit. *Bioinformatics* **2013**, *29*, 845−854.
(32) Schultz, A. J.; Kofke, D. A. Quantifying computational effort required for stochastic averages. *J. Chem. Theory Comput.* **2014**, *10*, 5229−5234.
(33) Kumar, S.; Rosenberg, J. M.; Bouzida, D.; Swendsen, R. H.; Kollman, P. A. The weighted histogram analysis method for free-energy calculations on biomolecules. I. The method. *J. Comput. Chem.* **1992**, *13*, 1011−1021.
(34) Roux, B. The calculation of the potential of mean force using computer simulations. *Comput. Phys. Commun.* **1995**, *91*, 275−282.
(35) Hub, J. S.; De Groot, B. L.; Van Der Spoel, D. g_wham: A Free Weighted Histogram Analysis Implementation Including Robust Error and Autocorrelation Estimates. *J. Chem. Theory Comput.* **2010**, *6*, 3713−3720.
(36) Shamov, G. A.; Schreckenbach, G.; Martin, R. L.; Hay, P. J. Crown ether inclusion complexes of the early actinide elements, [AnO2 (18-crown-6)] n^+, An= U, Np, Pu and n= 1, 2: A relativistic density functional study. *Inorg. Chem.* **2008**, *47*, 1465−1475.
(37) Guilbaud, P.; Wipff, G. Hydration of uranyl (UO_2^{2+}) cation and its nitrate ion and 18-crown-6 adducts studied by molecular dynamics simulations. *J. Phys. Chem.* **1993**, *97*, 5685−5692.
(38) Chen, B.; Wang, J.; Kong, L.; Mai, X.; Zheng, N.; Zhong, Q.; Liang, J.; Chen, D. Adsorption of uranium from uranium mine contaminated water using phosphate rock apatite (PRA): isotherm, kinetic and characterization studies. *Colloids Surf., A* **2017**, *520*, 612−621.
(39) Sun, Z.; Chen, D.; Chen, B.; Kong, L.; Su, M. Enhanced uranium (VI) adsorption by chitosan modified phosphate rock. *Colloids Surf., A* **2018**, *547*, 141−147.
(40) Belle, J. Oxygen and uranium diffusion in uranium dioxide (a review). *J. Nucl. Mater.* **1969**, *30*, 3−15.
(41) Awakura, Y.; Sato, K.; Majima, H.; Hirono, S. The Measurement of the Diffusion Coefficient of U(VI) in Aqueous Uranyl Sulfate Solutions. *Metall. Trans. B* **1987**, *18*, 19−23.
(42) Chopra, M.; Choudhury, N. Effect of uranyl ion concentration on structure and dynamics of aqueous uranyl solution: A molecular dynamics simulation study. *J. Phys. Chem. B* **2014**, *118*, 14373−14381.
(43) Choudhury, N.; Pettitt, B. M. Dynamics of Water Trapped between Hydrophobic Solutes. *J. Phys. Chem. B* **2005**, *109*, 6422−6429.
(44) Kommu, A.; Velachi, V.; Cordeiro, M. N. D. S.; Singh, J. K. Removal of Pb (II) Ion Using PAMAM dendrimer Grafted Graphene and Graphene Oxide Surfaces: A Molecular Dynamics Study. *J. Phys. Chem. A* **2017**, *121*, 9320−9329.
(45) Anitha, K.; Namsani, S.; Singh, J. K Removal of heavy metal ions using a functionalized single-walled carbon nanotube: a molecular dynamics study. *J. Phys. Chem. A* **2015**, *119*, 8349−8358.

DOI: 10.1021/acs.jced.9b00462
J. Chem. Eng. Data 2020, 65, 1051−1059